A suppression of differential rotation in Jupiter's deep interior

Tristan Guillot, Y. Miguel, B. Militzer, W. B Hubbard, Y. Kaspi, E. Galanti, H. Cao, R. Helled, S. M Wahl, L. Iess, et al.

A suppression of differential rotation in Jupiter's deep interior

T. Guillot[1], Y. Miguel[1], B. Militzer[2], W.B. Hubbard[3], Y. Kaspi[4], E. Galanti[4], H. Cao[5], R. Helled[6], S.M. Wahl[2], L. Iess[7], W.M. Folkner[8], D.J. Stevenson[5], J.I. Lunine[9], D.R. Reese[10], A. Biekman[1], M. Parisi[7], D. Durante[6], J.E.P. Connerney[11], S.M. Levin[8], S.J. Bolton[12]

[1]*Université Côte d'Azur, OCA, Lagrange CNRS, 06304 Nice, France*
[2]*University of California, Berkeley, CA 94720, USA*
[3]*Lunar and Planetary Laboratory, University of Arizona, Tucson, AZ 85721, USA*
[4]*Weizmann Institute of Science, Rehovot 76100, Israel*
[5]*California Institute of Technology, Pasadena, CA 91125, USA*
[6]*University of Zurich, 8057 Zurich, Switzerland*
[7]*Sapienza Università di Roma, 00184 Rome, Italy*
[8]*Jet Propulsion Laboratory, California Institute of Technology, Pasadena, CA 91109, USA*
[9]*Cornell University, Ithaca, NY 14853, USA*
[10]*LESIA, Observatoire de Paris, PSL Research University, CNRS, Sorbonne Universités, UPMC Univ. Paris 06, Univ. Paris Diderot, Sorbonne Paris Cité, 92195 Meudon, France*
[11]*NASA/GSFC, Greenbelt, Maryland, USA*
[12]*SwRI, San Antonio, Texas, USA*

The question of whether Jupiter's interior is differentially rotating has been a major puzzle[1,2], limiting our ability to probe the structure and composition of the planet[3,4]. The discovery by Juno that Jupiter's gravity field is north-south asymmetric[5] and the determination of its non-zero odd gravitational moments J_3, J_5, J_7 and J_9 demonstrates that the observed zonal flow must persist to a depth of about 3000 km[6]. Here, we show that beneath that layer, the planet rotates nearly as a rigid body with differential rotation decreasing by at least an order of magnitude compared to the atmosphere. Moreover, from the comparison of Jupiter's even moments J_4, J_6, J_8 and J_{10} as observed by Juno and as obtained by interior models, we find that the atmospheric zonal flow extends to more than 2000 km and to less than 3500 km, making it fully consistent with the constraints independently obtained from the odd gravitational moments. This depth corresponds to the point at which the electric conductivity becomes large and magnetic drag should suppress differential rotation[7]. Based on the dependence of electric conductivity with planetary mass, we expect the outer differentially-rotating region to be at least three times deeper in Saturn and shallower in massive giant planets and brown dwarfs.

Juno measurements of odd gravitational moments[5] constrain the maximum depth to which the observed atmospheric zonal flow persists[6]. These estimates, however, are based on the north-south asymmetries in the zonal flow, and cannot exclude the presence of a deeper north-south symmetrical flow. Fortunately, further insights can be obtained by comparing the even gravitational moments obtained from interior models assuming rigid rotation with those expected for a differentially-rotating planet. The moments from rigidly-rotating interior models are highly correlated because they probe similar regions of the interior[8]. On the other hand, differential rotation similar to that observed in the cloud layer puts weight relatively evenly in the different harmonics [9,10].

We derive an ensemble of interior models with Jupiter's mass and equatorial radius using both the CEPAM code[11] and by perturbing density profiles obtained by the CMS code[12]. Our range of J_2 values is set by Juno's measurements and the maximum uncertainty due to the unknown interior differential rotation[10]. These models use different equations of state of hydrogen and helium[13,14], including a possible jump of up

to 500 K in temperature in the helium phase-separation region, and the possibility (or not) of a dilute core[12]. The calculation of the gravitational moments is performed in two ways, directly with the CMS theory[15,16] or with a 4th order theory of figures (ToF)[17,18] combined with a direct integration of the reconstructed two-dimensional density structure using a Gauss-Legendre quadrature. A calibration of the values obtained from the ToF to the CMS values ensures an accurate estimate of the high order *J*s (see Methods).

The offset between differential and rigid rotation $\Delta J_{2i} = J_{2i}^{\text{differential}} - J_{2i}^{\text{rigid}}$ is calculated by assuming that the dynamical flows generate density perturbations that can be related through thermal wind balance[10,19]. We use a polynomial fit of degree *m* to the observed zonal winds[20] and an exponential decay in wind strength of e-folding depth *H*. We vary *m* between 2 and 30 and *H* between 0 (rigid rotation) and 100,000 km (rotation on cylinders all the way to the centre of the planet), thus creating a wide range of possible interior flows. We use the Juno measurements[5] to calculate effective gravitational moments $J_{2i}^{\text{eff}}(H,m) = J_{2i}^{\text{Juno}} - \Delta J_{2i}(H,m)$. These are the values that are to be matched by interior models assuming rigid rotation.

The gravitational moments obtained from interior models are compared to the effective gravitational moments in Fig. 1. Our interior models purposely cover a wide range of J_2 values, compatible with the Juno measurement and variable interior differential rotation, from a very shallow region with differential rotation at the surface to one extending to the planet's centre (upper left panel of fig. 1). We also allow for a wide range of meridional profiles (*m* values), allowing the possibility of the internal flows to vary substantially from the cloud-level wind profile, particularly having less latitudinal variation. We see that the extent of interior model solutions is significantly smaller in J_4 *vs.* J_6 and becomes a well-defined linear relation in J_6 *vs.* J_8, and J_8 *vs.* J_{10}. On the other hand, differential rotation affects the J_{2i} values more uniformly as a function of the parameters *H* and *m*. The solutions are obtained by matching rigidly-rotating interior models (black and grey dots) to the effective gravitational moments (coloured squares).

In the J_2 *vs.* J_4 plane, any value of the effective gravitational moments can be matched by small adjustments of the assumed interior composition: no constraint on

interior differential rotation is possible. In the J_4 *vs.* J_6, J_6 *vs.* J_8, and J_8 *vs.* J_{10} planes, the same interior models are incompatible with most values of the effective gravitational moments. The corresponding values of H and m are therefore excluded. In the J_4 *vs.* J_6 plane, the interior models cross the Juno point, providing only an upper limit on H. However, in the J_6 *vs.* J_8, and J_8 *vs.* J_{10} planes, the slight offset between the Juno point and the interior model area implies that a lower limit on H may be derived. Mechanisms other than differential rotation cannot realistically explain that offset: in order to alter the relations between J_6, J_8, and J_{10}, they would need to affect significantly the interior density profile in the outer ~30% of the planet[8]. In this region, uncertainties in the H-He phase separation and related composition jumps are included in the interior model and constrained by the J_4 *vs.* J_6 values. The other source of uncertainty is related to the condensation of water and silicates but is expected to only affect J_4 by about 10^{-7}, J_6 by 10^{-8} and J_8 by ~10^{-9}, i.e., more than one order of magnitude less than required (see Methods).

In order to estimate possible values of the wind depth H, we calculate the likelihood that an atmospheric model (accounting for the effect of differential rotation) combined with an interior model (accounting for the effect of interior structure) matches the observed even gravity coefficients. For a given value of H, we integrate the function $exp[-(J_{2i}^{eff}(H,m)- J_{2i}^{model})^2/(2\sigma_{2i}{}^2)]/[(2\pi)^{1/2}\ \sigma_{2i}]$ over all models in our ensemble and all values of m. σ_{2i} encompasses the 1σ uncertainty of the Juno measurements as well as the variance in our ensemble of models. Figure 2 confirms the analysis of Fig. 1 that J_2 *vs.* J_4 or J_4 *vs.* J_6 alone cannot be used to constrain the wind depth, H. The strongest constraints on H come from the J_6 *vs.* J_8 and J_8 *vs.* J_{10} planes because the weights of atmospheric contributions become large relative to those for the lower harmonics. When constraints from J_2 to J_{10} are combined, a strong peak emerges in the likelihood function in Fig. 2. Only values of H between 2000 and 3500 km are compatible with the available data. This depth corresponds to the one at which the electrical conductivity[21] increases to a modest value (0.01 – 1 S/m) and the Lorentz force associated with the zonal flow (magnetic drag) becomes comparable to the observed divergence of the Reynolds stress in the cloud layers[7,22,23]. Indeed, energy budget considerations of the Ohmic dissipation being smaller than the observed luminosity predict a penetration depth between about 2000 and 2800 km below the cloud tops of Jupiter [7,24].

The results obtained in Figs. 1 and 2 are based on a simple law (an exponential decay of the atmospheric zonal flow) that was obtained independently of Juno's measurements[10]. In Fig. 3 we show that the more elaborate differential-rotation law that is fitted to Jupiter's odd gravitational moments[6] is consistent with the interior models, confirming that both the symmetric and asymmetric part of the observed zonal flow extend to a similar depth. The solutions matching the observations generally cover an extensive parameter space in Extended Data Table 1. One salient feature is that they are characterized by an increase of the heavy elements abundance in the deeper interior, either where hydrogen becomes metallic or deeper as a dilute core, confirming the results obtained after Juno's first two orbits[12].

Furthermore, by adopting the differential rotation law for the upper 3000 km, we can provide approximate constraints on the rotation of the deeper parts of the planet. In order to do so, we assume that the deeper interior rotates on cylinders all the way to the center and adopt a scaled version of the ΔJ_{2i} relations from Fig. 1. We calculate the likelihood of such a model with unknown deep differential rotation v between 0 and the observed atmospheric one (~100 m/s), using the same approach as for Fig. 2 (see Methods). The results are shown in Extended Data Fig. 2. Only an upper limit may be derived on v: Beneath the first 3000km layer, deep differential rotation must be limited to amplitudes at least an order of magnitude smaller than the observed atmospheric ones.

The observed winds thus penetrate deep in the atmosphere all the way to the levels where the conductivity and the resulting magnetic drag become large enough[7,23,24]. In gaseous planets, electrical conductivity strongly increases with pressure, which is itself a strong function of the planetary mass. In Saturn, one must go three times deeper than in Jupiter to reach the same conductivity[7,21]. The planet has a similar intrinsic luminosity but a magnetic field that is an order of magnitude smaller[25]. We hence expect Saturn's outer differentially-rotating region to extend to at least 9000 km, which

should leave a strong imprint on its gravity field. Conversely, massive giant exoplanets and brown dwarfs should have shallower differentially-rotating outer envelopes[26].

References

1. Busse, H.F. A simple model of convection in the Jovian atmosphere. *Icarus*, **29**, 255-260 (1976)
2. Vasavada, A.R. & Showman, A.P. Jovian atmospheric dynamics: an update after Galileo and Cassini. *Reports on Progress in Physics*, Volume 68, Issue 8, pp. 1935-1996 (2005)
3. Hubbard, W. B. Effects of differential rotation on the gravitational figures of Jupiter and Saturn. *Icarus*, **52**, 509–515 (1982).
4. Guillot, T., Gautier, D. & Hubbard, W.B. NOTE: New Constraints on the Composition of Jupiter from Galileo Measurements and Interior Models. *Icarus*, **130**, 534-539 (1997)
5. Iess, L. et al. The asymmetric gravity field of Jupiter. *Nature*, this issue (2017)
6. Kaspi, Y. et al. Jupiter's deep atmosphere revealed by Juno's asymmetric gravity measurements. *Nature*, this issue (2017)

7. Cao, H., & Stevenson, D. J. Zonal flow magnetic field interaction in the semi-conducting region of giant planets. *Icarus* **296**, 59-72 (2017)

8. Guillot, T. THE INTERIORS OF GIANT PLANETS: Models and Outstanding Questions. *Ann. Rev. Earth Plan. Sci.* **33**, 493-530 (2005)

9. Hubbard, W. B. NOTE: Gravitational Signature of Jupiter's Deep Zonal Flows. *Icarus* **137**, 357-359 (1999)

10. Kaspi, Y., et al. The effect of differential rotation on Jupiter's low-degree even gravity moments. *Geophys. Res. Let.* **44**, 5960-5968 (2017)

11. Miguel, Y., Guillot, T., & Fayon, L. Jupiter internal structure: the effect of different equations of state. *Astron. Astrophys.* **596**, A114 (2016)

12. Wahl, S. M., et al. Comparing Jupiter interior structure models to Juno gravity measurements and the role of an expanded core. *Geophys. Res. Let.* **44**, 4649-4659 (2017)

13. Militzer B. & Hubbard W. B. Ab Initio Equation of State for Hydrogen-Helium Mixtures with Recalibration of the Giant-planet Mass-Radius Relation. *Astrophys. J.* **774** 148 (2013).

14. Becker, A., Lorenzen, W., Fortney, J. J., et al. Ab Initio Equations of State for Hydrogen (H-REOS.3) and Helium (He-REOS.3) and their Implications for the Interior of Brown Dwarfs. *Astrophys. J. Suppl.* **215**, 21 (2014)

15. Hubbard W. B. Concentric Maclaurin Spheroid Models of Rotating Liquid Planets. *Astrophys. J.* **768**, 43 (2013)

16. Wisdom, J. & Hubbard, W. B. Differential rotation in Jupiter: A comparison of methods. *Icarus* **267**, 315-322 (2016)

17. Zharkov, V. N. & Trubitsyn, V. P. Physics of planetary interiors. Astronomy and Astrophysics Series, Tucson: Pachart (1978)

18. Nettelmann, N. Low- and high-order gravitational harmonics of rigidly rotating Jupiter. *A&A* **606**, A139 (2017)

19. Kaspi, Y., Showman, A. P., Hubbard, W. B., Aharonson, O., & Helled, R. Atmospheric confinement of jet streams on Uranus and Neptune. Nature **497**, 344-347 (2013)

20. Ingersoll, A.P., Dowling, T.E., Gierasch, P.J., Orton, G.S., Read, P.L., Sánchez-Lavega, A., Showman, A.P., Simon-Miller, A.A. & Vasavada, A.R. Dynamics of Jupiter's atmosphere. In *Jupiter. The planet, satellites and magnetosphere*. Edited by Fran Bagenal, Timothy E. Dowling, William B. McKinnon. Cambridge planetary science, Vol. 1, Cambridge, UK: Cambridge University Press, ISBN 0-521-81808-7, 2004, p. 105 - 128

21. French, M., Becker, A., Lorenzen, W., Nettelmann, N., Bethkenhagen, M., Wicht, J., & Redmer, R. Ab Initio Simulations for Material Properties along the Jupiter Adiabat. *Astrophys. J. Suppl.* **202**, 5 (2012)

22. Salyk, C., Ingersoll, A. P., Lorre, J., Vasavada, A., & Del Genio, A. D. Interaction between eddies and mean flow in Jupiter's atmosphere: Analysis of Cassini imaging data. *Icarus* **185**, 430-442 (2006)

23. Schneider, T., & Liu, J. Formation of Jets and Equatorial Superrotation on Jupiter. *JAtS* **66**, 579-(2009)

24. Liu, J., Goldreich, P. M., & Stevenson, D. J. Constraints on deep-seated zonal winds inside Jupiter and Saturn. *Icarus* **196**, 653-664 (2008)

25. Connerney, J.E.P. (2015). Planetary magnetism. Volume 10: Planets and Satellites. In G. Schubert and T. Spohn, (Eds.) *Treatise in Geophysics*, Elsevier, Oxford, UK, vol. 10.06, 195-237.

26. Showman, A. P., & Guillot, T. Atmospheric circulation and tides of ``51 Pegasus b-like" planets. *A&A* **385**, 166-180 (2002)

Acknowledgments

The research described in this paper was carried out at the Observatoire de la Côte d'Azur under the sponsorship of the Centre National d'Etudes Spatiales; at the Jet Propulsion Laboratory, California Institute of Technology, under a contract with NASA; by the Southwest Research Institute under contract with NASA; at the Weizmann Institute of Science under contract with the Israeli Space Agency. Computations were performed on the 'Mesocentre SIGAMM' machine, hosted by the Observatoire de la Côte d'Azur.

Authors contributions

T.G., Y.M. and B.M. ran interior models of Jupiter and carried the analysis. W.B.H. and A.B. compared gravitational moments obtained by different methods. E.G. and Y.K. calculated the offset introduced by differential rotation. H.C. R.H, D.J.S and J.I.L. provided theoretical support. S.M.W. provided additional interior models of Jupiter. D.R.R. provided a routine to calculate efficiently high order gravitational moments. W.M.F., M.P. and D.D. carried out the analysis of the Juno gravity data. J.E.P.C., S.M.L., S.J.B. supervised the planning, execution, and definition of the Juno gravity experiment.

Competing interests

The authors declare that they have no competing financial interests.

Correspondence

Reprints and permissions information is available at npg.nature.com/reprintsandpermissions. Correspondence and requests for materials should be addressed to T. Guillot (email:tristan.guillot@oca.eu).

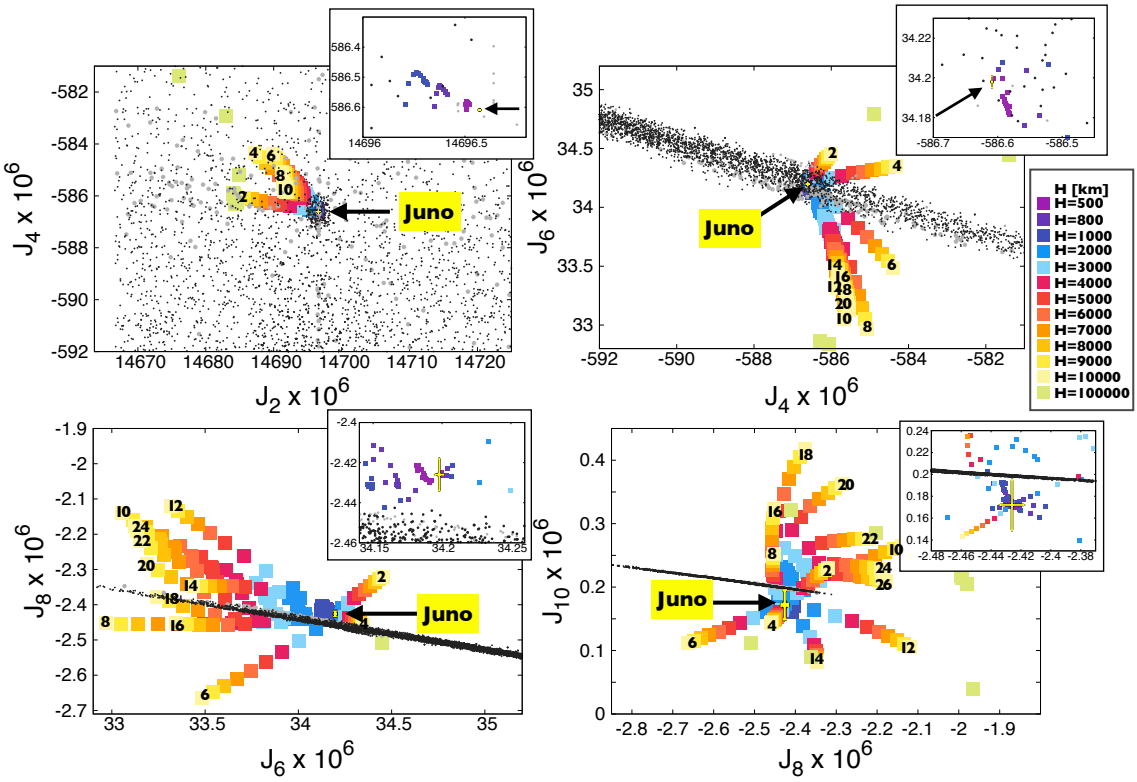

Fig. 1. Jupiter's gravitational moments J_2 to J_{10}. The Juno determinations are shown in yellow with 1σ error bars. The points correspond to interior models of Jupiter calculated assuming rigid rotation using CEPAM[11] (black points) and CMS[12,15] (grey points). The coloured squares correspond to the values to be reproduced by interior models for observed zonal flows extending to various depths, from H=500 km to H=100,000 km, and by filtering the atmospheric flow (m from 2 to 30– see text)[10]. The numbers on the plots correspond to the value of m for H=10,000 km.

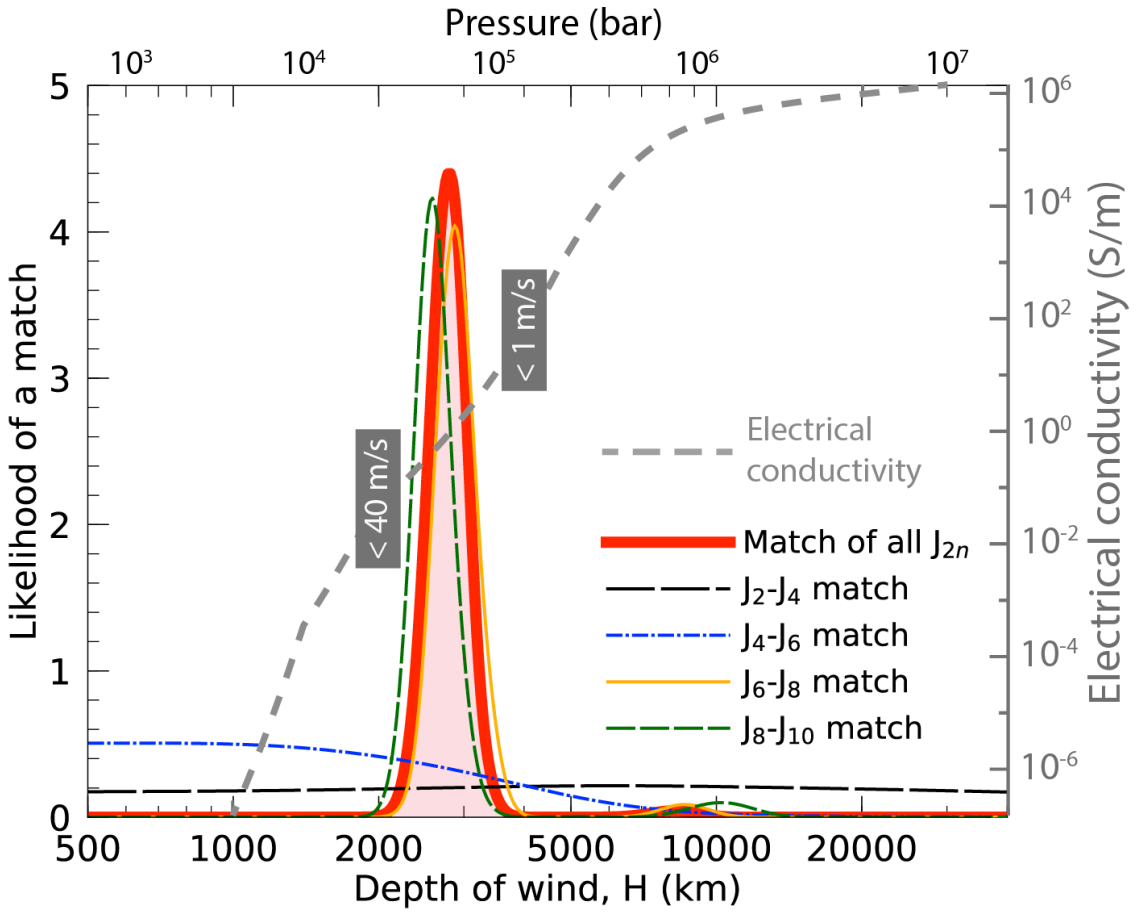

Fig. 2. Constraint on the depth H of Jupiter's zonal flow obtained from interior models and Juno's even gravitational moments. The lines correspond to the four panels of fig. 1: J_2 vs. J_4, J_4 vs. J_6, J_6 vs. J_8, and J_8 vs. J_{10}. The profile of electrical conductivity in Jupiter's interior[21] is shown for comparison. Ohmic dissipation is expected to limit zonal flows to less than 40 m/s at a depth of 2000 km and 1 m/s at 4000 km[7]. Only interior models with $-586.8 < J_4 \times 10^6 < -584.5$ (corresponding to the maximum range of J_4^{eff} values allowed by differential rotation) were included in the calculation.

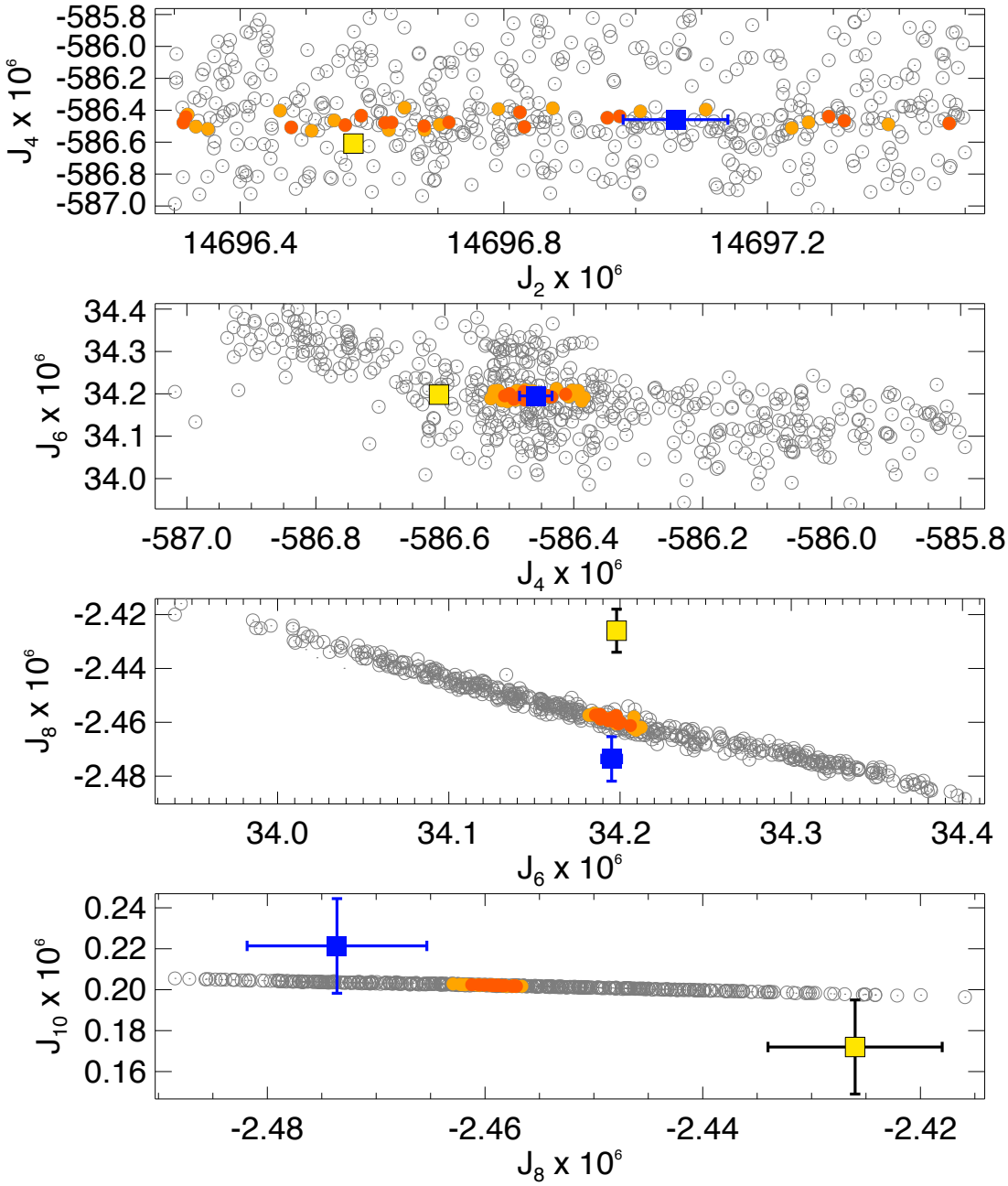

Fig. 3. Ensemble of interior models of Jupiter fitting the gravitational moments J_2 to J_{10}. The Juno values are shown as yellow squares with error bars. The blue squares with error bars correspond to the effective gravitational moments obtained when accounting for the differential rotation derived from the Juno odd gravitational moments[6]. Interior

models fitting all effective gravitational moments J_4 to J_{10} (blue squares) are highlighted in colour depending on whether they fit within 2σ (orange) or 3σ (light orange).

Methods

Calculation of interior models.

The internal structure of Jupiter is calculated using the equations of hydrostatic equilibrium, energy transport, energy and mass conservation, which are solved with the interior structure code CEPAM[27]. These models are constructed to fit observational constrains such as Jupiter's radius and gravitational moments.

We adopt a four-layer structure for the interior models: (1) a helium-poor upper envelope in which hydrogen is in molecular form, (2) a helium-rich, metallic-hydrogen lower envelope, (3) a dilute core which consists of helium-rich metallic hydrogen with an increase of the heavy element content and (4) a central dense core of ices and rocks. Because convection tends to homogenize large fractions of the envelope[28], we expect that regions (1) and (2) should be largely convective and homogeneous. However, the presence of a phase separation of helium in metallic hydrogen at ~1 Mbar[29] may create a barrier to convection[30,31,32] and thus yield an increase in both helium and heavy element abundances. The dilute core region may be inhomogeneous and an extension of the core itself [33,34].

The determination of Jupiter internal structure still rests on the accuracy of the equations of state[11,35,36]. For H and He we use two of the most recently published equations of state calculated from ab initio simulations: MH13[13] and REOS3[14]. For REOS3-H and REOS3-He, the pure hydrogen and pure helium EOS tables, respectively, we calculate the entropy with a dedicated procedure[11]. MH13 was made for a fixed mixture of H and He. To allow different concentrations of H and He in the different layers we extracted from this table the table for H and since MH13 does not cover all the pressure range in Jupiter's interior we merge this one with the SCvH equation of state[11,35]. The heavy elements are assumed to be composed of rocks and ices[36].

Since we attempt to calculate the largest possible ensemble of realistic interior models we allow for the possibility of either efficient convection or double-diffusive convection in the helium phase separation region by including a possible jump in temperature in that region [30,31,32,37]. Uncertainties in the location and characteristics of

the helium phase separation zone are considered by varying the limit between region (1) and region (2) between 0.8 and 3 Mbar[29]. Uncertainties in the presence of the dilute core region (3) are included by performing a fraction of the calculations either without this region (three-layer models), or, with it and including three variable parameters: the location of the transition, its smoothness, and the heavy element fraction in the transition region.

In order to obtain this large ensemble of possible interior models, for each set of imposed parameters, we obtain the mass fraction of ices in region (1) and the core mass that best fit the observed equatorial radius of the planet, 71,492 ± 4 km[38] and the gravitational moment J_2 following an optimisation procedure[39]. We do not attempt to fit the other gravitational moments and we allow for a large range of values for J_2 between 0.014665 and 0.014725 in order to probe the ensemble of possible solutions, from rigidly-rotating solutions to differential rotation extending all the way to the planetary centre.

Extended Data Table 1 summarizes the parameters used in the models. Their values are drawn either from a Gaussian distribution when they are constrained observationally, or from a uniform distribution when we do not have sufficient a priori knowledge of their value. More than 200,000 interior models were calculated.

We calculate models in which the amount of water and rocks are suppressed at temperatures below 200K and 3000K, respectively, in order to mimic the condensation of these species. The changes on J_4 ($\sim 10^{-7}$), J_6 ($\sim 10^{-8}$) and J_8 ($\sim 10^{-9}$) are found to be too small to affect the results.

We also use an alternative method in which we perturb the density profiles for Jupiter[9] and calculate their gravitational moments using CMS. We introduce between 1 and 4 density jumps at random pressures. The magnitudes of the density changes are also chosen randomly between +/- 5% to represent possible compositional deviations or EOS deviations that are not yet understood. These thus represent a wide ensemble of models –some of them being unphysical (e.g., because of a decrease in density with increasing pressure). Yet, the inferred ensemble of gravitational moments (grey points in fig. 1) overlaps very closely with that obtained using full interior structure models

(black points) suggesting that the results, in terms of the gravitational moments of a rigidly rotating Jupiter, are robust.

Calculation of gravitational moments

The calculation of the gravitational moments is performed as follows: For the CMS model and their perturbations we use the concentric MacLaurin spheroid approach (CMS) [15,16]. For the CEPAM models, we use the faster theory of figures (ToF) to 4th order [17,18] to obtain a bi-dimensional interior density profile ρ(ζ,θ) where ζ is the (dimensionless) mean radius and θ the colatitude. We then calculate the gravitational moments J_ℓ as:

$$J_\ell = -\frac{1}{MR^\ell}\int_0^1\int_0^{2\pi}\int_0^{\pi} r^\ell \rho(\zeta,\theta)P_\ell(\cos\theta)r^2\left|r_\zeta\right|\sin\theta\,\mathrm{d}\theta\mathrm{d}\Phi\mathrm{d}\zeta$$

where M and R are the planetary mass and equatorial radius, respectively, r_ζ the partial derivative of r with respect to ζ, and $P_\ell(\cos\theta)$ is the Legendre polynomial of degree ℓ. We use a Gauss-Legendre quadrature in the horizontal direction (θ,ϕ) and finite differences in the radial direction (ζ).

Extended Data Table 2 shows a comparison of solutions obtained from this method and from two other approaches. First, we use CEPAM on an n=1 polytropic EOS and compare the solution to that calculated with an extremely accurate method[16]. The results are in good agreement, with offsets being at most $1.5\text{x}10^{-7}$. These offsets are a natural consequence of the ToF expansion[17,18]. We then compare more realistic Jupiter models calculated with CEPAM and with the CMS method. The offsets for high order moments are remarkably similar to the ones obtained for the polytropic model. The offsets for J_2 are comparatively more important and are believed to be due to discretization errors[16]. These imply a small error on the core mass and mass of heavy elements in the planet by an amount that is negligible in regard to the other uncertainties[18]. By comparing the solutions obtained with two slightly different models which have the same J_2 value with CEPAM and CMS, respectively (line REOS1a-1b in Extended Data Table 2), we can see that the offset in J_2 has a limited consequence on J_4 and an even smaller one on higher order moments.

Based on these results, we adopt the following offsets δJ_4=0.11x10^{-6}, δJ_6=-0.057x10^{-6}, δJ_8=0.166x10^{-6}, δJ_{10}=-0.029x10^{-6}. Although we expect this offset to change slightly as a function of the parameters used, the level of precision obtained is sufficient to derive constraints on the internal differential rotation. This is shown in Extended Data Fig. 1 which compares calculations performed with the different approaches.

Constraints on deep differential rotation

In order to derive constraints on the amount of differential rotation underneath the "atmospheric" layer, we proceed as follows: First we imagine that we can divide the interior into a differentially-rotation outer shell tied to the atmospheric zonal wind and a deeper layer with a smaller amount of differential rotation (with characteristic zonal velocity v) all the way to the centre. Given that the rotation of the outer shell is constrained by the odd harmonics, we wish to find the possible values of v. We therefore need to associate effective gravitational moments $J_{2k}^{\rm obs}$ to each v.

We do so by adding Juno's value, the offset derived from the latitude-dependent flow profile that best fits Juno's odd moments, and a deeper component that is obtained from the purely cylindrical component for H=100,000 km (see fig. 1)[10]:

$$J_{2k}^{\rm obs} = J_{2k}^{\rm Juno} - \delta J_{2k}^{\rm oddfit} - \frac{v}{100{\rm m/s}}\delta J_{2k}^{H=100{,}000\ {\rm km}}(m)$$

where we assume that the value of δJ_{2k} obtained for the atmospheric zonal flows (v~100m/s) may be scaled linearly for any characteristic velocity v.

We then calculate the likelihood of these models as a function of v with the same approach as for Fig. 2, including all gravitational moments J_4 to J_{10}. The results are plotted in Extended Data Fig. 2. For our preferred model, we obtain a strong upper limit at 10 m/s with a preference for smaller values of v. For v<6 m/s the best interior models are found to lie within two standard deviations of all effective gravitational moments. For comparison, a model with a thin weather layer (H=0) and differential rotation on cylinders to the center with velocity v is found to also favour small value of v<10 m/s but is incompatible with Juno's gravitational moments.

Code availability

The CEPAM code is available for download from the following url:
https://svn.oca.eu/codes/CEPAM/trunk

Data availability

Data sharing is not applicable to this article as no datasets were generated during the current study.

References

27. Guillot, T., & Morel, P. 1995, *A&AS* **109**, 109-123

28. Vazan, A., Helled, R., Podolak, M., & Kovetz, A. The Evolution and Internal Structure of Jupiter and Saturn with Compositional Gradients. *Astrophys. J.* **829**, 118 (2016)

29. Morales, M. A., Hamel, S., Caspersen, K., & Schwegler, E. Hydrogen-helium demixing from first principles: From diamond anvil cells to planetary interiors. *PhRvB* **87**, 174105-(2013)

30. Stevenson, D. J., & Salpeter, E. E. The dynamics and helium distribution in hydrogen-helium fluid planets. *Astrophys. J. Suppl.* **35**, 239-261 (1977)

31. Nettelmann, N., Fortney, J. J., Moore, K., & Mankovich, C. An exploration of double diffusive convection in Jupiter as a result of hydrogen-helium phase separation. *MNRAS* **447**, 3422-3441 (2015)

32. Mankovich, C., Fortney, J. J., & Moore, K. L. Bayesian Evolution Models for Jupiter with Helium Rain and Double-diffusive Convection. *Astrophys. J.* **832**, 113-(2016) Stevenson, D. J. Cosmochemistry and structure of the giant planets and their satellites. *Icarus* **62**, 4-15 (1985)

33. Helled, R., & Stevenson, D. The Fuzziness of Giant Planets' Cores. *Astrophys. J.* **840**, L4 (2017)

34. Hubbard, W. B., & Militzer, B. A Preliminary Jupiter Model. *Astrophys. J.* **820**, 80-(2016)

35. Saumon, D., Chabrier, G., & van Horn, H. M. An Equation of State for Low-Mass Stars and Giant Planets. *Astrophys. J. Suppl.* **99**, 713-(1995)

36. Saumon, D., & Guillot, T. Shock Compression of Deuterium and the Interiors of Jupiter and Saturn. *Astrophys. J.* **609**, 1170-1180 (2004)

37. Leconte, J., & Chabrier, G. A new vision of giant planet interiors: Impact of double diffusive convection. *A&A* **540**, A20 (2012)

38. Lindal, G. F. The atmosphere of Neptune - an analysis of radio occultation data acquired with Voyager 2. *AJ* **103**, 967-982 (1992)

39. Guillot, T. A comparison of the interiors of Jupiter and Saturn. *P&SS* **47**, 1183-1200 (1999)

40. Seiff, A., et al. Thermal structure of Jupiter's atmosphere near the edge of a 5-micron hot spot in the north equatorial belt. *JGR* **103**, 22857-22890 (1998)

41. Serenelli, A. M., & Basu, S. Determining the Initial Helium Abundance of the Sun. *Astrophys. J.* **719**, 865-872 (2010)

42. von Zahn, U., Hunten, D. M., & Lehmacher, G. Helium in Jupiter's atmosphere: Results from the Galileo probe helium interferometer experiment. JGR ***103***, 22815-22830 (1998)

EXTENDED DATA

Extended Data Table 1: Parameters used for the calculation of interior models

Parameter	Description	Type	Mean	σ or ΔX
T_{1bar}	1 bar temperature, from Voyager and Galileo measurements [38,40]	Gaussian	165K	4K
$Y_{proto}/(X_{proto}+Y_{proto})$	Protosolar helium mixing ratio obtained from solar models [41]	Gaussian	0.277	0.006
$Y_{atm}/(X_{atm}+Y_{atm})$	Helium mixing ratio in Jupiter's atmosphere as measured by the Galileo probe [42]	Gaussian	0.238	0.005
P_{He}	Characteristic pressure of the helium phase separation region [29,31]	Uniform	1.9 Mbar	1.1 Mbar
ΔT_{He}	Temperature increase over the helium phase separation region [12]	Uniform	0	500 K
$L_{dilcore}$	Presence of the diluted core region	Binary	0/1	
$P_{dilcore}$	Pressure of the diluted core region	Uniform	21.5 Mbar	18.5 Mbar
$\Delta \log P_{dilcore}$	Smoothness of the diluted core transition	Uniform	0.0255	0.0245
$\Delta Z_{dilcore}$	Mass mixing ratio increase in the diluted core region	Uniform	0.2	0.2
$Z_{ices}^{(1)}$	Mass mixing ratio of ices in region (1)	Fitted		
$Z_{rocks}^{(1)}$	Mass mixing ratio of rocks in region (1)	Uniform	0.025	0.025
ΔZ_{ices}	Jump in the mass mixing ratio of ices from region (1) to region (2)	Uniform	0.075	0.075
ΔZ_{rocks}	Jump in the mass mixing ratio of rocks from region (1) to region (2)	Uniform	0.075	0.075
M_{core}	Mass of the central dense core	Fitted		

Extended Data Table 2: Comparison of model gravitational moments

Model	Method	$J_2\times10^6$	$J_4\times10^6$	$J_6\times10^6$	$J_8\times10^6$	$J_{10}\times10^6$	$J_{12}\times10^6$
Polytrope	CEP	13988.65	-531.8675	30.06605	-1.98248	0.14772	-0.01201
	WH16	13988.51	-531.8281	30.11832	-2.13212	0.17407	-0.01568
	CEP-WH16	0.14	-0.0394	-0.05227	0.14964	-0.02635	0.00367
REOS1a	CEP	14696.72	-587.8227	34.22564	-2.29778	0.17296	-0.01413
	CMS	14690.66	-587.3989	34.26170	-2.46234	0.20218	-0.01821
	CEP-CMS	6.06	-0.4238	-0.03606	0.16456	-0.02922	0.00408
REOS1b	CEP	14702.78	-588.1331	34.24635	-2.29937	0.17309	-0.01414
	CMS	14696.72	-587.7090	34.28245	-2.46399	0.20232	-0.01822
	CEP-CMS	6.06	-0.4240	-0.03610	0.16462	-0.02923	0.00408
REOS1a-1b	CEP-CMS	-0.00	-0.1136	-0.05681	0.16621	-0.02936	0.00409
MH13	CEP	14695.97	-590.2377	34.46524	-2.31752	0.17465	-0.01428
	CMS	14690.96	-589.9033	34.51000	-2.48443	0.20422	-0.01841
	CEP-CMS	5.01	-0.3343	-0.04476	0.16691	-0.02957	0.00413

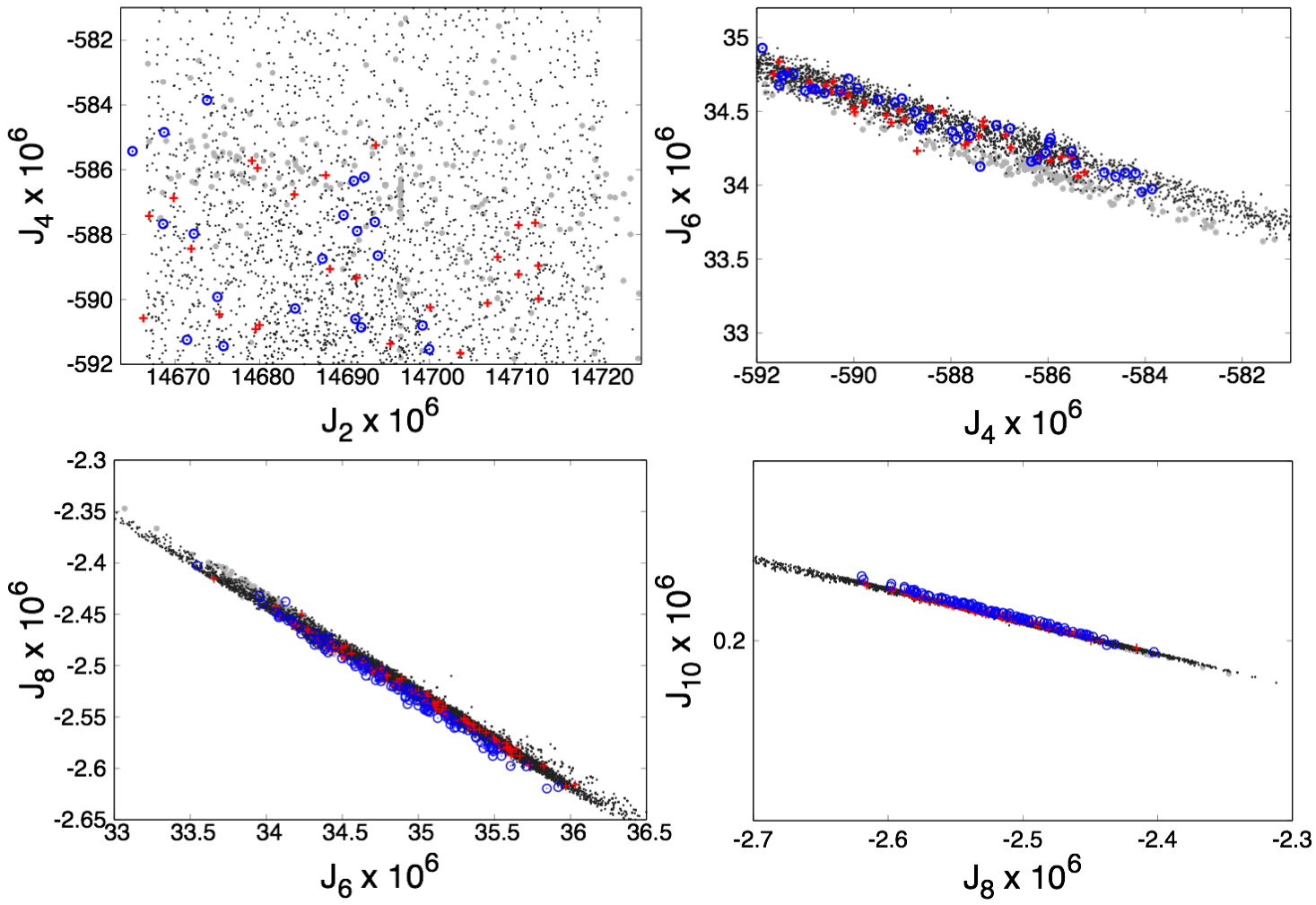

Extended Data Fig. 1. Validation of the calculation of gravitational moments with the CEPAM method. The four panels provide a comparison of gravitational moments J_2 to J_{10} calculated with various methods: CEPAM models with 241 radial layers (black points), CMS models with 800 layers (grey points), CEPAM models with 1041 layers (red crosses), and CMS calculations for the CEPAM models with 1041 layers (blue circles).

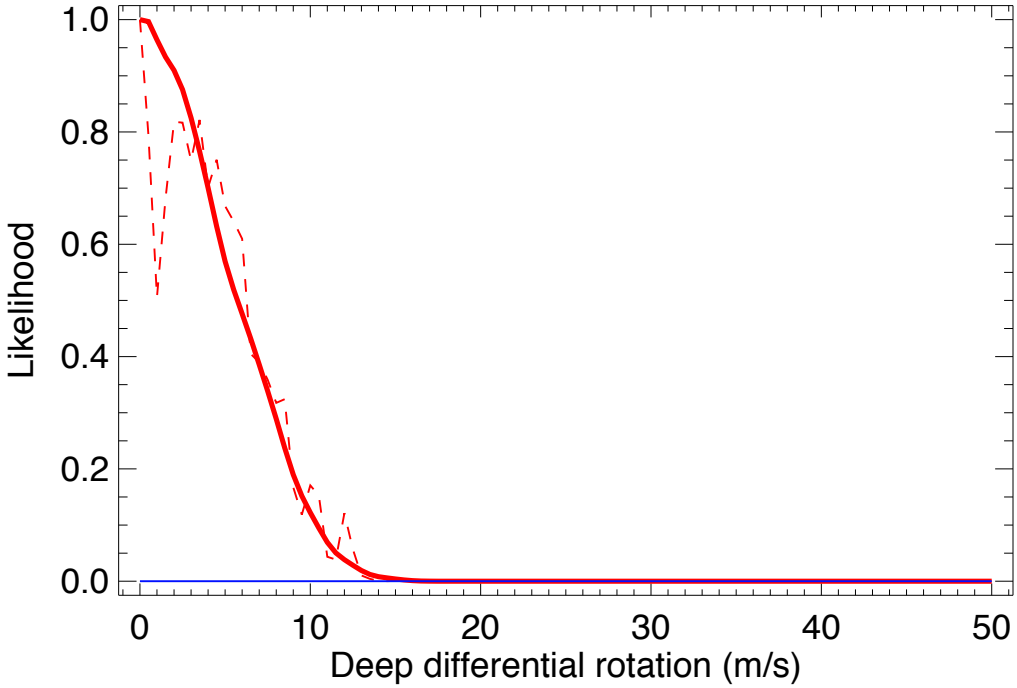

Extended Data Figure 2: Constraint on the characteristic amplitude of deep differential rotation in Jupiter. The red curves show the likelihood of models in which we add to the differentially-rotating outer region constrained by Juno's odd moments[6] a deeper cylindrical flow of amplitude v. The dashed red curve uses 1σ error bars. The plain red curve considers an extended ensemble of possibilities for the outer flow[6] with solutions up to 3σ. In both cases, the model favours v<6 m/s. The blue curve shows the same model but without the added outer layer. That model also favours low-amplitude winds but is found to be 4×10^4 times less likely.

WEB PART

Nature requirements (words):		Present version
Introductory paragraph:	200~300	206
Main text	1500	~1406
References	< 30	25
Method section	3000	~1405
References Total	<50	41